WIND TURBINES - A PRIMER

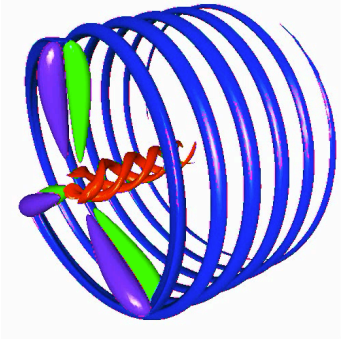

WIND TURBINES - A PRIMER

Topics covered

1. Wind turbine types
2. Key parameters and dimensionless groups, expected power delivery
3. Actuator disk models, the Betz limit and other optima
4. Horizontal axis wind turbines
   a. Blade aerodynamics
   b. Blade element method
5. Electrical generator characteristics
6. Control of HAWT

Texts

1. *Wind Energy Explained*, 2e, Manwell, McGowan & Rogers, Wiley 2009 — Online PDFs
2. *Wind Energy Handbook*, Burton, Sharpe, Jenkins & Bossanyi, Wiley 2001 — Online PDFs
3. *Aerodynamics of Wind Turbines*, Hansen, Earthscan 2008 — Online PDFs
4. *Small Wind Turbines*, Wood, Springer 2011 — Online PDFs
5. *Principles of Helicopter Aerodynamics*, 2e, Leishman, Cambridge 2006

Key parameters and dimensionless groups

Wind turbines extract kinetic energy from a flow of air; the rate at which this could be extracted is the available aerodynamic power

$$\frac{KE}{\Delta t} \propto \tfrac{1}{2}\dot{m}V_\infty^2 = \tfrac{1}{2}\rho A V_\infty^3 = P_{\text{av}} \qquad \text{NB: } P_{\text{av}} \propto V_\infty^3 \qquad \dot{m} \propto \rho A V_\infty$$

Typically $A = \pi R^2 = \pi D^2/4$ where R is maximum rotor radius.

The power extraction produces a thrust load on the turbine $T \propto \dot{m}V_\infty \propto \tfrac{1}{2}\rho A V_\infty^2$

Turbine blade tip speed is ΩR where Ω is the shaft angular speed.

Three key overall dimensionless performance parameters are (similar to most rotating fluid machines)

1. Power coefficient $C_P = \dfrac{P_{\text{shaft}}}{\frac{1}{2}\rho A V_\infty^3}$

2. Thrust coefficient $C_T = \dfrac{T}{\frac{1}{2}\rho A V_\infty^2}$

3. Tip speed ratio $\lambda = \dfrac{\Omega R}{V_\infty}$

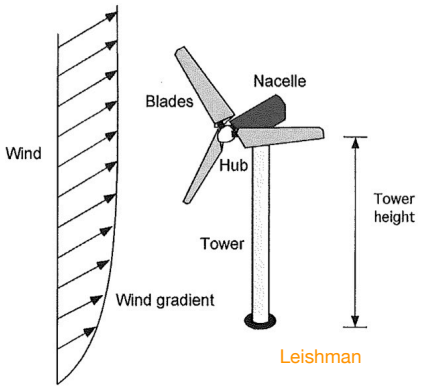

Many other dimensionless groups are important too, including

- Rotor plane yaw angle to incident wind direction, γ
- Pitch angle of blades relative to rotor plane, θ
- Blade airfoil lift and drag coefficients, C_l, C_d

Also, ratio of tower height to boundary layer depth, etc., etc.

Primary wind turbine types

	Horizontal Axis (HAWT)		Vertical Axis (VAWT)	
Lift-based	 Propeller-type	**Large**	 Darrieus rotor	*Lift-based*
Lift-based	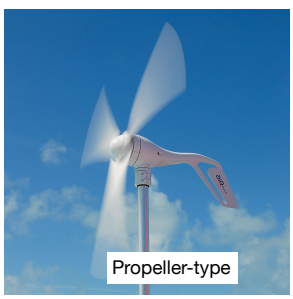 Propeller-type	**Small**	 Savonius rotor	*Drag-based*

Wind turbine types

Like most turbo-machinery, different wind turbine types are most efficient at different dimensionless speeds (tip speed ratio).

Generally, HAWT propeller types are the most aerodynamically efficient but that is not always the most important consideration.

The most efficient turbines rely on extracting power via lift forces on blades, rather than drag forces.

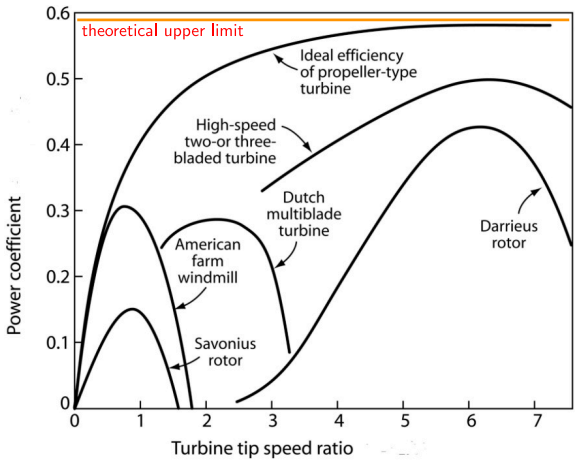

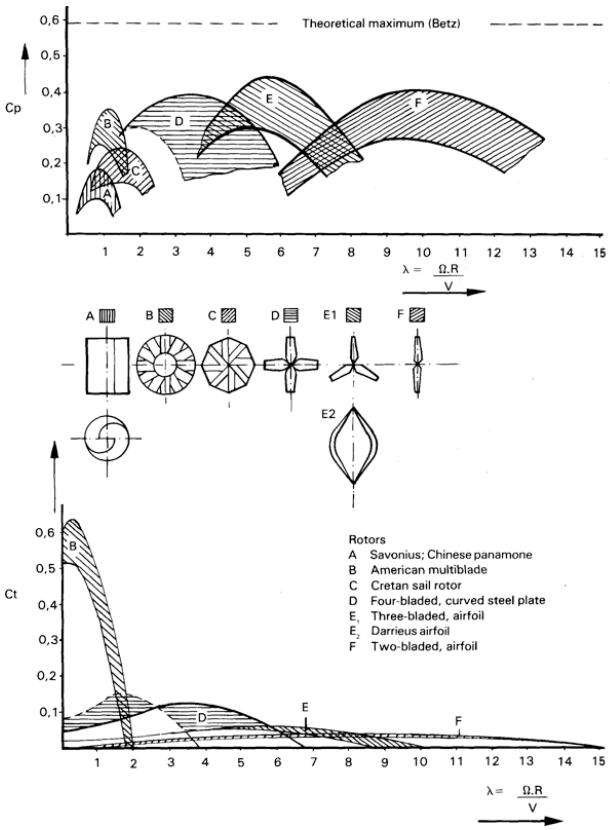

Operating characteristics

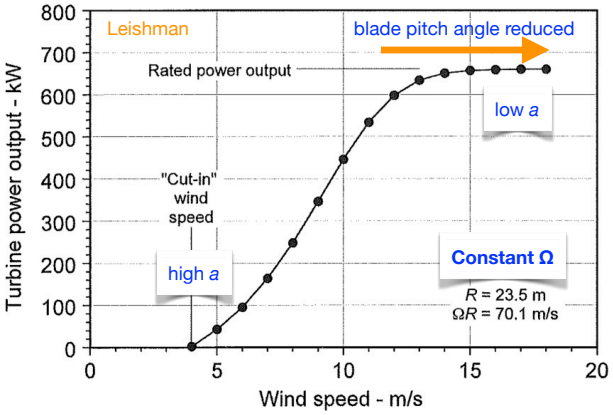

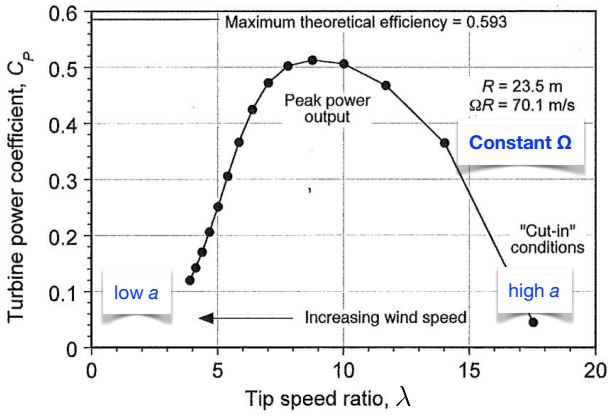

Typically, turbines do not rotate below a fixed 'cut-in' wind speed: below this, blades are stalled and electrical windage losses are high.

Above cut-in, power output increases approximately like V^3 until the rated power output is reached. Then, various strategies may be used to limit the power output.

For constant rotational speed, peak efficiency is only achieved over a small range of wind speeds: variable speed is more typical for large machines.

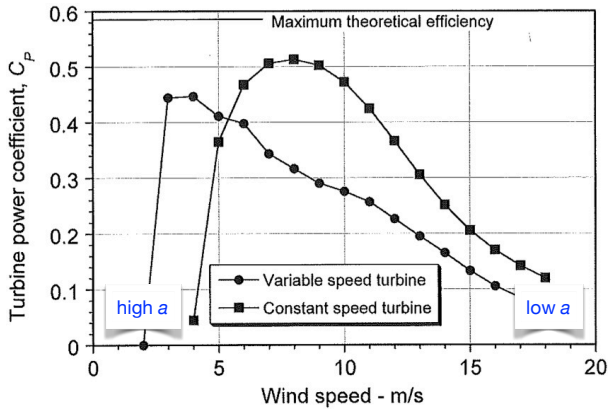

Expected power output

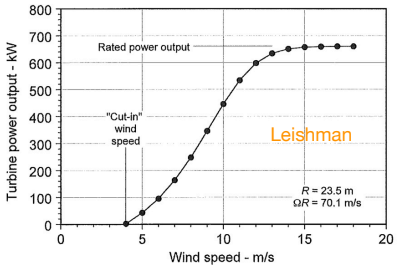

Given the turbine operating characteristics as a function of wind speed

$$P = P(V_\infty)$$

and the probability density function (PDF) of wind speeds <u>at the turbine location and rotor shaft height</u>

$$p(V_\infty), \quad \text{with} \quad \int_0^\infty p(V_\infty)\,\mathrm{d}V_\infty = 1$$

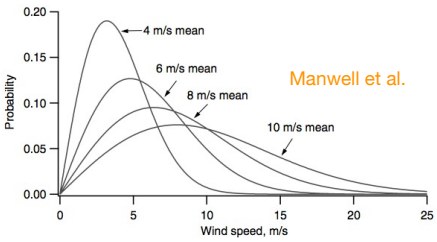

the expected average power output is

$$\overline{P} = \int_0^\infty P(V_\infty)\,p(V_\infty)\,\mathrm{d}V_\infty$$

The **capacity factor** (maximum value 1) is then

$$CF = \frac{\overline{P}}{\text{Rated Power}} \qquad \text{(Typically < 0.5.)}$$

<u>Annual expected energy output</u>

$$\overline{W} = \overline{P} \times 365 \times 24 = CF \times \text{Rated Power} \times 365 \times 24 \qquad \text{(Units e.g. kWh.)}$$
$$= CF \times \text{Rated Power} \times 8760$$

Clearly, good characterisation of the wind speed PDF at the actual turbine location is fundamental to accurate estimation of average power output.

Yaw, pitch and speed regulation

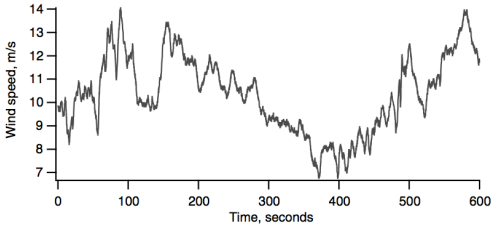

The natural wind typically is quite variable in both speed and direction over a range of both length and time scales.

This has implications for control as well as expected power output.

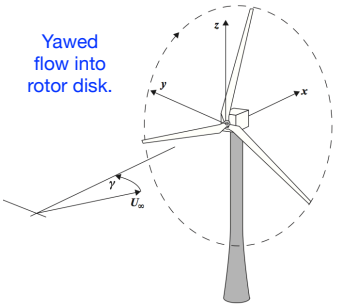

<u>Wind speed variation – *pitch*</u>

The aim is to run a turbine at its optimal tip speed ratio λ.

This typically leads us to control blade pitch angle, though speed regulation of generator output characteristic is another option.

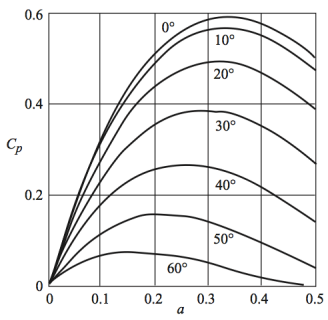

<u>Directional variation – *yaw*</u>

HAWT do not naturally align themselves to the local wind direction and so (a) the disk is usually yawed w.r.t. the current wind direction and (b) some form of active yaw control/regulation is required.

Unsurprisingly, yaw reduces the effective power output and also leads to elevated fatigue loading.

Simple theory says that $C_{P,\max,\gamma} = C_{P,\max}\cos^3\gamma$

Actuator disk model – 1

The 'actuator disk' model takes an idealised control-volume-based approach to wind turbine performance estimation and provides the upper limit estimate.

It ignores details of flow through the rotor, as well as swirl in the wake, and may be used to represent the limiting performance of 'any' wind turbine class.

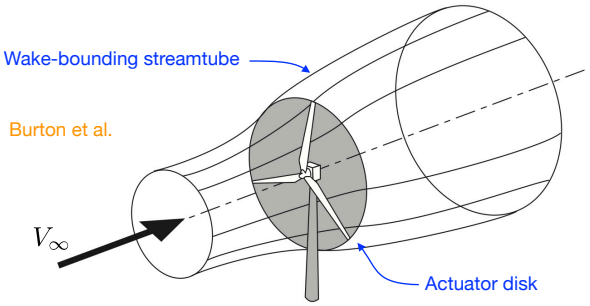

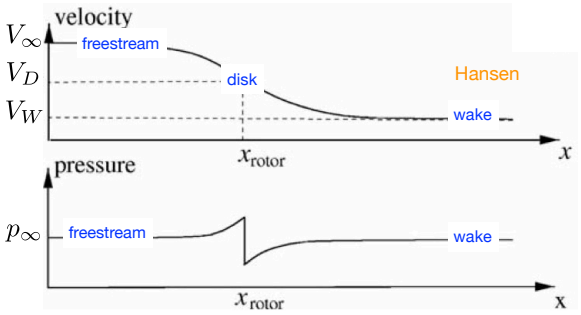

Consider an axisymmetric control volume *CV* bounded by control surface *CS*.

The actuator disk is excised from *CV* and *CS* is partitioned into the union

$S = S_I \cup S_C \cup S_{TP} \cup S_D$

T: thrust exerted by rotor on fluid in *CV*.

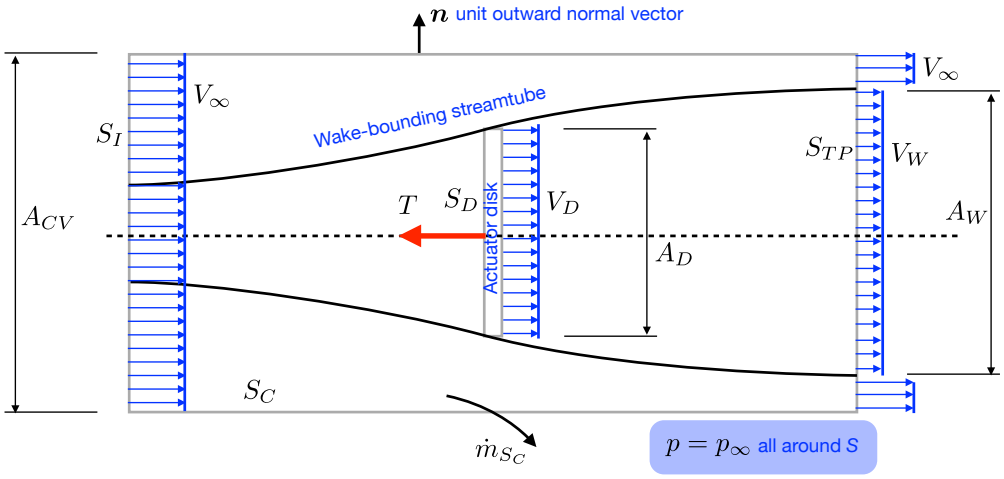

Actuator disk model – 2

We take the flow to be (a) steady in time (b) incompressible, (c) inviscid and (d) bounded by a time-invariant control surface.

Geometric integral over S $\oint \boldsymbol{n}\,\mathrm{d}S = \boldsymbol{0}$

Integral statement of mass conservation $\oint \boldsymbol{V}\cdot\boldsymbol{n}\,\mathrm{d}S = 0$ using $\rho = \text{const.}$

Integral statement of momentum conservation $\cancel{\int \frac{\partial}{\partial t}(\rho\boldsymbol{V})\,\mathrm{d}V}^{\text{steady}} + \oint \rho\boldsymbol{V}\boldsymbol{V}\cdot\boldsymbol{n}\,\mathrm{d}S = \Sigma\boldsymbol{F}_{CV}$

'Momentum flux out – momentum flux in = force acting on control volume.'

There are no net pressure forces on far-field boundary since the pressure is uniform there. Forces acting on boundary segment S_D are summarised as ***T***, the (negative of the) thrust acting on the rotor.

$$\rho\oint \boldsymbol{V}\boldsymbol{V}\cdot\boldsymbol{n}\,\mathrm{d}S = \boldsymbol{T} \quad \text{or, just for the axial component:} \quad \rho\oint V_x\boldsymbol{V}\cdot\boldsymbol{n}\,\mathrm{d}S = -T$$

Partition outer integral, use fact that the net momentum contribution over S_D is zero:

$$\rho\oint \boldsymbol{V}\boldsymbol{V}\cdot\boldsymbol{n}\,\mathrm{d}S = \rho\int \boldsymbol{V}\boldsymbol{V}\cdot\boldsymbol{n}\,\mathrm{d}S_I + \rho\int \boldsymbol{V}\boldsymbol{V}\cdot\boldsymbol{n}\,\mathrm{d}S_C + \rho\int \boldsymbol{V}\boldsymbol{V}\cdot\boldsymbol{n}\,\mathrm{d}S_{TP}$$

$$= \rho V_\infty^2 A_{CV} + \rho V_\infty\int \boldsymbol{V}\cdot\boldsymbol{n}\,\mathrm{d}S_C + \rho[V_\infty^2(A_{CV}-A_W) + V_W^2 A_W]$$

Now $\int \boldsymbol{V}\cdot\boldsymbol{n}\,\mathrm{d}S_C = \dot{m}_{S_C}/\rho = V_\infty A_{CV} - V_\infty(A_{CV}-A_W) - V_W A_W = (V_\infty - V_W)A_W$

Actuator disk model – 3

Substituting back and rearranging we find $\rho V_W A_W (V_\infty - V_W) = T$ Good, but too many unknowns.

Try using continuity and Bernoulli equations as well.

Since $\rho V_W A_W$ is the mass flow rate inside the streamtube, this can also be written $\dot{m}(V_\infty - V_W) = T$

where $\dot{m} = \rho V_W V_W = \rho V_D A_D$

Now the rotor thrust could also be written as $T = \Delta p A_D$ where $\Delta p = p_+ - p_-$ pressure difference across disk

Using Bernoulli's equation from inlet up to the actuator disk and then downstream of the disk to the exit

$p_\infty + \frac{1}{2}\rho V_\infty^2 = p_+ + \frac{1}{2}\rho V_D^2$ and $p_- + \frac{1}{2}\rho V_D^2 = p_\infty + \frac{1}{2}\rho V_W^2$ giving $\Delta p = p_+ - p_- = \frac{1}{2}\rho(V_\infty^2 - V_W^2)$

Equating the two expressions for thrust we have $\rho A_D V_D (V_\infty - V_W) = \frac{1}{2}\rho A_D (V_\infty^2 - V_W^2)$

Solving for V_D we get $V_D = \frac{1}{2}(V_\infty + V_W)$ i.e. the average of the upstream and downstream speeds.

If we define $V_D = (1-a)V_\infty$ where *a* is the 'axial induction factor' and then further rearranging the above we find $V_W = (1-2a)V_\infty$ i.e. half the slow-down occurs upstream, half downstream of the disk.

Finally $T = 2\rho A_D V_\infty^2 a(1-a)$ or, compared to the maximum available dynamic pressure force on the disk

$$C_T = \frac{T}{\frac{1}{2}\rho V_\infty^2 A_D} = 4a(1-a)$$

Integral statement of energy conservation

$$\cancel{\dot{Q}}^{\text{no heat}} - \dot{W} = \frac{\mathrm{d}E_{SYS}}{\mathrm{d}t} = \int \cancel{\frac{\partial}{\partial t}}^{\text{steady}}(e\rho)\,\mathrm{d}V + \oint e\rho \boldsymbol{V}\cdot\boldsymbol{n}\,\mathrm{d}S$$

'Heat rate in – Power out = net outflow of energy per unit time.'

Actuator disk model – 4

with *e* being energy per unit mass: $e = \cancel{e_{\text{internal}}} + e_{\text{kinetic}} + \cancel{e_{\text{potential}}} + \cancel{e_{\text{other}}}$ and $e_{\text{kinetic}} = \frac{1}{2}\rho V^2$

So $-\dot{W} = \oint \frac{1}{2}\rho V^2 \boldsymbol{V}\cdot\boldsymbol{n}\,\mathrm{d}S$ where $\dot{W} = \dot{W}_{\text{shaft}} + \dot{W}_{\text{press}} + \dot{W}_{\text{viscous stress}}$

$$= P_{\text{shaft}} + \oint p\boldsymbol{V}\cdot\boldsymbol{n}\,\mathrm{d}S - \oint \boldsymbol{\tau_n}\cdot\boldsymbol{V}\,\mathrm{d}S$$

ignoring the final term for frictionless steady flow,

$$-P_{\text{shaft}} = \cancel{\oint p\boldsymbol{V}\cdot\boldsymbol{n}\,\mathrm{d}S} + \oint \frac{1}{2}\rho V^2 \boldsymbol{V}\cdot\boldsymbol{n}\,\mathrm{d}S$$

since $p = p_\infty = \text{const}$ on control surface and $\oint \boldsymbol{V}\cdot\boldsymbol{n}\,\mathrm{d}S = 0$ for incompressible flow

$$-P_{\text{shaft}} = \underbrace{-\tfrac{1}{2}\rho V_\infty^3 A_{CV}}_{\text{on } S_I} + \underbrace{\tfrac{1}{2}\rho V_\infty^3 (A_{CV} - A_W)}_{\text{on } S_{TP}} + \underbrace{\tfrac{1}{2}\rho V_W^3 A_W + \tfrac{1}{2}\rho V_\infty^2 (V_\infty - V_W) A_W}_{\text{on } S_C}$$

$$= +\tfrac{1}{2}\rho V_W^3 A_W - \tfrac{1}{2}\rho V_\infty^2 V_W A_W$$

$$= \dot{m}(\tfrac{1}{2}V_W^2 - \tfrac{1}{2}V_\infty^2) \qquad \text{Recall } \dot{m} = \rho V_W A_W = \rho V_D A_D$$

Finally $P_S = \frac{1}{2}\rho A_D V_D (V_\infty^2 - V_W^2) = 2\rho A_D V_\infty^3 a(1-a)^2$

or, normalising by the maximum possible kinetic energy flow rate through disk area

$$C_P = \frac{P_S}{\frac{1}{2}\rho V_\infty^3 A_D} = 4a(1-a)^2$$

The Betz limit

From the actuator disk model

$C_T = 4a(1-a)$ max value where $\dfrac{\mathrm{d}C_T}{\mathrm{d}a} = 0 \implies a = 0.5, \quad C_{T_{\max}} = 1$

$C_P = 4a(1-a)^2$ max value where $\dfrac{\mathrm{d}C_P}{\mathrm{d}a} = 0 \implies a = 1/3, \quad C_{P_{\max}} = \dfrac{16}{27} = 0.593$

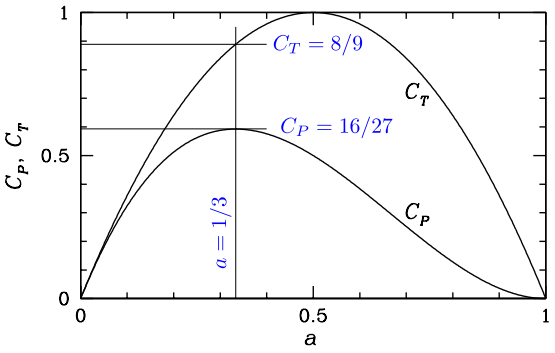

In practice, the simple actuator disk model is only found to work for $a < 0.4$.

Note that in this range, wake expansion increases with a, with the ratio of upstream to downstream streamtube areas being $1 - 2a$.

Also note that the simple actuator disk model is also appropriate for use with propellers.

$C_{P,\max} = 0.593$ is known as the Betz limit, and no unshrouded wind turbine has exceeded it.

It is often used in estimating the upper limits of possible power extraction for a given wind turbine (not restricted to HAWT).

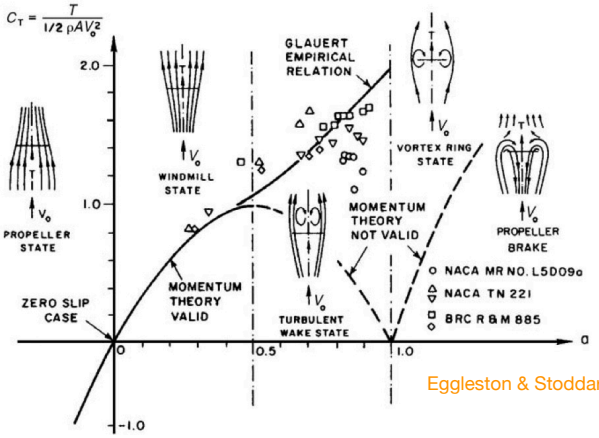

Eggleston & Stoddard

Actuator disk with swirl – 1

Our analysis so far takes no account of the fact that because power results from torque (i.e. the product of a tangential force) multiplied by a rotational speed there must be an equal and opposite tangential force applied to the fluid at each radial location, causing a swirl in the fluid. This contributes kinetic energy in the wake that cannot be recovered, and the more swirl, the greater the loss.

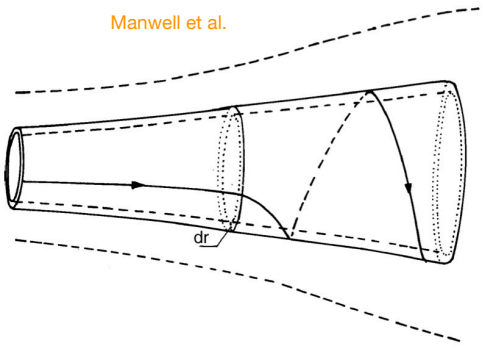

Manwell et al.

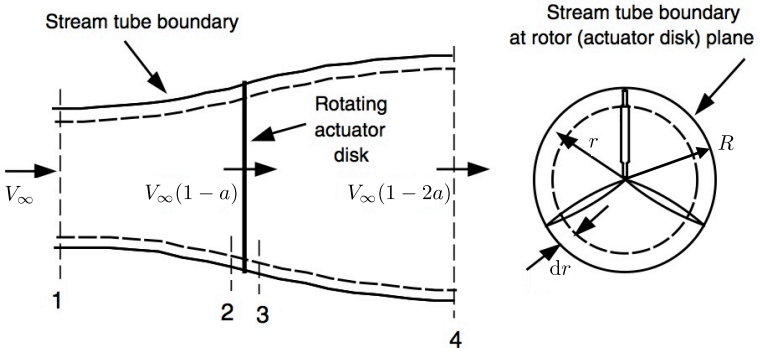

Also to this point, we have not accounted for the influence of tip speed ratio on power. The following analysis tells us the best we could hope to achieve by way of power output at different tip speed ratios, and describes conditions in the “Optimum Glauert rotor”.

Note that although swirl is accounted for, individual blades are not; the analysis is still for an actuator disk model.

Somewhat paradoxically, it transpires that the lowest wake swirl occurs for high tip speed ratios.

Actuator disk with swirl – 2

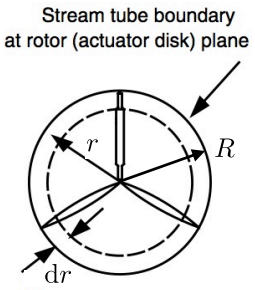

From conservation of linear momentum one finds the infinitesimal contribution to overall thrust at each radial location is

$$\mathrm{d}T = \mathrm{d}(\dot{m})(V_\infty - V_W) = 4a(1-a)\tfrac{1}{2}\rho V_\infty^2 2\pi r\,\mathrm{d}r = 4\pi r\rho V_\infty^2 a(1-a)\,\mathrm{d}r$$

From conservation of angular momentum one finds the infinitesimal contribution to overall power at each radial location is

$$\mathrm{d}P = \mathrm{d}(\dot{m})\Omega r V_\theta = 2\pi r^2 \rho V_D \Omega V_\theta\,\mathrm{d}r \qquad \left(= \Omega\,\mathrm{d}Q \quad \text{where dQ is infinitesimal contribution to rotor torque}\right)$$

where Ω is rotational speed and V_θ is the absolute swirl velocity downstream of the rotor disk (zero swirl upstream). As before V_D is the axial velocity at the disk.

Recall that $V_D = (1-a)V_\infty$ and we also define $V_\theta = 2a'\Omega r$ where *a* and *a'* are respectively axial and azimuthal (or swirl) induction factors. Note that *a* and *a'* vary along the blade radius.

So now $\mathrm{d}P = 4\pi\rho\Omega^2 V_\infty a'(1-a)r^3\,\mathrm{d}r$ and $P = 4\pi\rho\Omega^2 V_\infty \int_0^R a'(1-a)r^3\,\mathrm{d}r$

In dimensionless terms $C_P = \dfrac{8}{\lambda^2}\int_0^\lambda a'(1-a)\lambda_r^3\,\mathrm{d}\lambda_r$ where tip speed ratio $\lambda = \dfrac{\Omega R}{V_\infty}$ and $\lambda_r = \dfrac{\Omega r}{V_\infty} = \lambda\dfrac{r}{R}$ dimensionless radial position for a given tip speed ratio

Clearly, in order to maximise C_P we need to maximise $a'(1-a)$, a function of radial position.

For potential (inviscid) flow and for small blade angles of attack we can relate the two induction factors *a'* and *a*. Various methods can produce the required relationship.

The geometrical method outlined here is based on the idea that the total induced velocity is in the same direction as the lift vector acting on a blade.

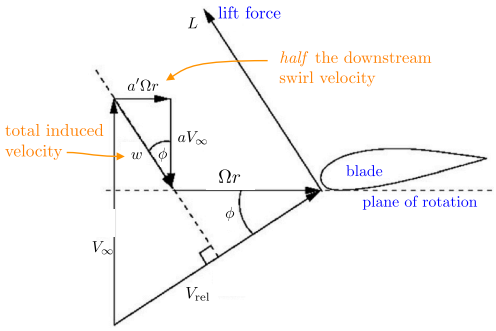

Actuator disk with swirl – 3

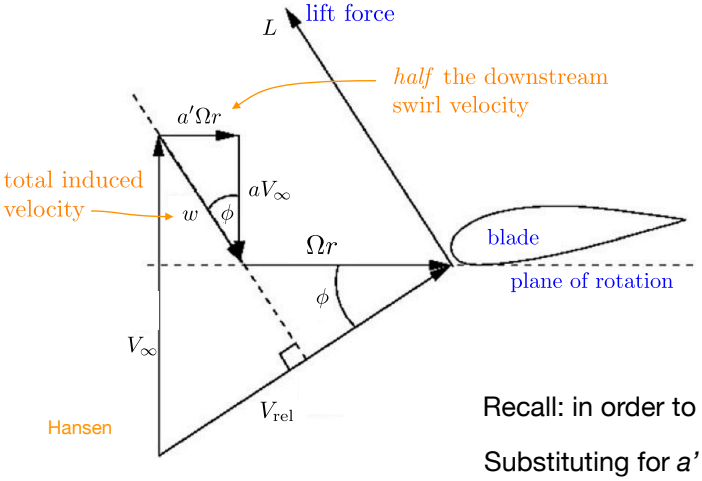

From similar triangles:

$$\tan\phi = \frac{a'\Omega r}{aV_\infty} \quad \text{and} \quad \tan\phi = \frac{(1-a)V_\infty}{(1+a')\Omega r}$$

Equate and rearrange:

$$\lambda_r^2 a'(1-a') = a(1-a) \qquad \lambda_r = \lambda r/R$$

or $$a' = -\frac{1}{2} + \frac{1}{2}\sqrt{1 + \frac{4}{\lambda_r^2}a(1-a)}$$

Recall: in order to maximise C_P we need to maximise $a'(1-a)$.

Substituting for *a'* and differentiating w.r.t. *a*, set to 0, we obtain

$\lambda_r^2 = \dfrac{(1-a)(4a-1)^2}{1-3a}$ and then $a' = \dfrac{1-3a}{4a-1}$ which are values that provide maximum power production.

Differentiating the first of these w.r.t. *a*, rearranging: $2\lambda_r \mathrm{d}\lambda_r = [6(4a-1)(1-2a)^2/(1-3a)^2]\mathrm{d}a$

Subbing back into $C_P = \dfrac{8}{\lambda^2}\int_0^\lambda a'(1-a)\lambda_r^3\,\mathrm{d}\lambda_r$ one obtains $\lambda = \dfrac{(1-a_2)(4a_2-1)^2}{1-3a_2}$

$$C_{P,\max} = \frac{24}{\lambda^2}\int_{a_1}^{a_2}\left[\frac{(1-a)(1-2a)(1-4a)}{1-3a}\right]^2 \mathrm{d}a$$

Where a_1 corresponds to the (root) axial induction factor for $\lambda_r = 0$ and a_2 corresponds to the (tip) axial induction factor for $\lambda_r = \lambda$.

Now from $\lambda_r^2 = \dfrac{(1-a)(4a-1)^2}{1-3a}$ and $\lambda = \dfrac{(1-a_2)(4a_2-1)^2}{1-3a_2}$ we see $\lambda_r = 0 \implies a_1 = 1/4$

$\lambda \to \infty \implies a_2 \to 1/3$

Actuator disk with swirl – 4

so that $$C_{P,\max} = \frac{24}{\lambda^2}\int_{1/4}^{a_2(\lambda)} \left[\frac{(1-a)(1-2a)(1-4a)}{1-3a}\right]^2 \mathrm{d}a$$ is only a function of λ.

By change of variables from (1 – 3*a*) to *x,* Glauert obtained the solution in closed form as

$$C_{P,\max} = \frac{8}{729\lambda^2}\left[\frac{64}{5}x^5 + 72x^4 + 124x^3 + 38x^2 - 63x - 12\ln x - 4x^{-1}\right]_{x=1-3a_2}^{x=1/4}$$

λ	a_2	$C_{P,\max}$
0.5	0.2983	0.289
1.0	0.3170	0.416
1.5	0.3245	0.477
2.0	0.3279	0.511
2.5	0.3297	0.533
5.0	0.3324	0.570
7.5	0.3329	0.581
10.0	0.3330	0.585
∞	1/3	0.593

For given λ, find optimal a_2 (the tip value of *a*), from which we can obtain *a'* at the tip and then all the way to the blade root.

We see that the Betz limit is recovered as

$$\lambda \to \infty$$

Turbines with these characteristics are called "optimal Glauert rotors".

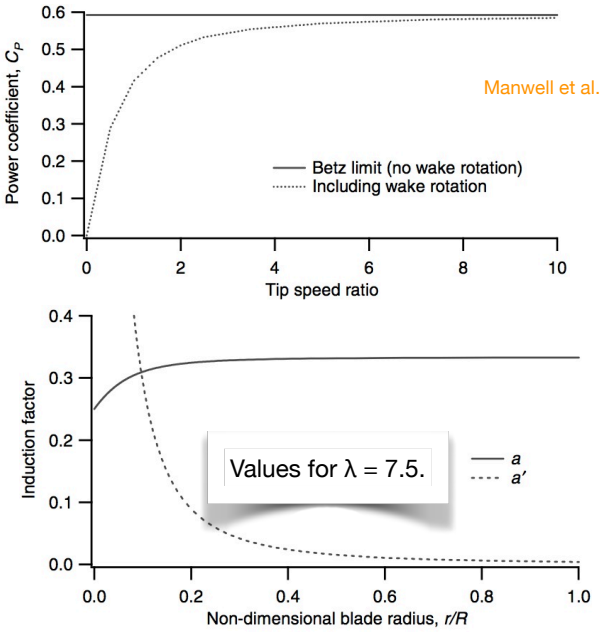

Blades, airfoils, wings

Turbine blades are basically rotating wings, usually twisted from root to tip in order to account for the difference in azimuthal blade speed from root to tip.

To make further progress in our analysis, we have to start considering blade aerodynamics and details of the flow around (a finite number of) blades, rather than assuming ideal flow in an actuator disk.

Since blades are typically long and thin and radial flows are typically small, it is usual to start out considering 2D flows around airfoils, and then add in 3D effects as corrections (but in which radial flow components are still ignored) . This is also true of most wing analysis and design, so the methodologies are firmly related.

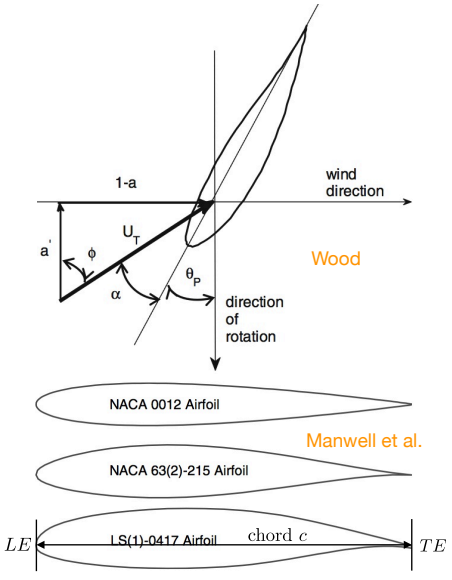

Fortunately (in the case of wings at least) the 3D effects are readily and accurately computable using inviscid/ideal aerodynamics, while flows around airfoils need to be characterised either by experimental measurements or nonlinear (i.e. boundary layer or Navier–Stokes) computations. For wind turbines, a full accounting for 3D effects is more complicated than is typical for wings, but simplified approaches are usually considered good enough for initial estimations.

When it comes to the flow around wind turbine airfoils, it is also fortunate that typical flow speeds are well below the speed of sound (about 340 m/s at sea level) so that compressibility effects are small – flows can be treated as incompressible, and the main parameters (in smooth flow) for airfoil performance are angle of attack α and chord Reynolds number.

$$Re = \frac{\rho V c}{\mu} = \frac{V c}{\nu}$$

Forces and moments on airfoils

Here all the forces and the pitching moment M_x are values per unit length along the span.

The overall reaction force ***R*** can be decomposed into various orthogonal components, here (*L*,*D*) and (*N*,*A*).

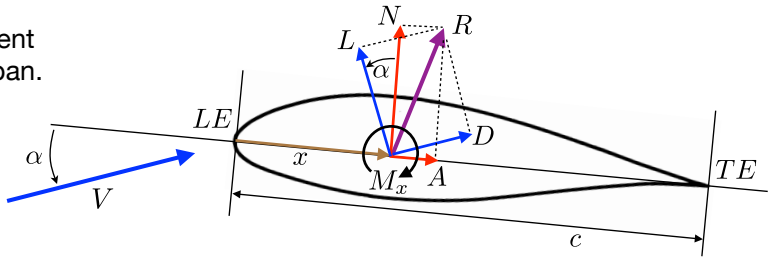

The forces and moments result from the integration of surface tractions around the perimeter of the airfoil. Again the surface tractions are conveniently decomposed into orthogonal components normal and tangential to the local perimeter.

Local: pressure and skin friction (tractions)

Local unit surface normal and tangential vectors ***n*** and ***t***.

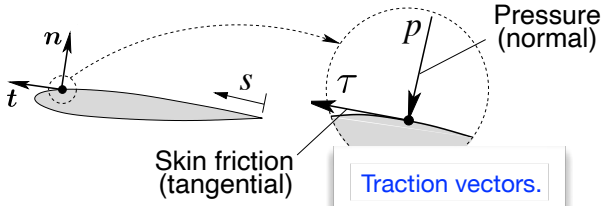

NB: one can show that for solid boundaries, the normal traction is caused only by pressure and the tangential traction only by viscous stress.

Global: lift, drag, and pitching moment

$$\boldsymbol{R} = \int_0^l (-p\boldsymbol{n} + \tau\boldsymbol{t})\,\mathrm{d}s$$

$$L = |\boldsymbol{R}|\cos\alpha$$

$$D = |\boldsymbol{R}|\sin\alpha$$

$$\boldsymbol{M} = \int_0^l (\boldsymbol{x}(s) - \boldsymbol{x}_0) \times (-p\boldsymbol{n} + \tau\boldsymbol{t})\,\mathrm{d}s \qquad (\boldsymbol{x}_0 \text{ is arbitrary})$$

Since typically *L* is what we want and *D* is an unwanted cost, desire $L \gg D$. Usually this also requires α to be fairly small, say < 15°.

NB: forces ***R***, *L* and *D* do not depend on choice of origin, but moment *M* does.

Aerodynamic coefficients

	Local/sectional	Global/wing/vehicle
Pressure coefficient	$C_p = \frac{p - p_\infty}{\frac{1}{2}\rho V_\infty^2}$	
Skin friction coefficient	$C_f = \frac{\tau}{\frac{1}{2}\rho V_\infty^2}$	
Lift force coefficient	$C_l = \frac{L}{\frac{1}{2}\rho V_\infty^2 c}$	$C_L = \frac{L}{\frac{1}{2}\rho V_\infty^2 S}$ S is the wing area
Drag force coefficient	$C_d = \frac{D}{\frac{1}{2}\rho V_\infty^2 c}$	$C_D = \frac{D}{\frac{1}{2}\rho V_\infty^2 S}$
Moment coefficient	$C_m = \frac{M}{\frac{1}{2}\rho V_\infty^2 c^2}$	$C_M = \frac{M}{\frac{1}{2}\rho V_\infty^2 S\bar{c}}$ $\bar{c}$ is the mean aerodynamic chord

↑ forces and moments here are per unit span length.

NB: by convention, lower-case subscripts (C_l etc.) denote sectional (2D) values while upper-case subscripts (C_L etc.) denote whole-aircraft (or 3D) values.

These global values are not very relevant to wind turbines owing to effects of blade twist and rotation.

Dimensional analysis shows that for 2D steady flow

$$C_i = \text{function}(\text{shape}, \alpha, Ma_\infty, Re_c); \quad i = p, f, l, d, m$$

$$Ma_\infty = V_\infty / a \qquad a = \text{speed of sound}$$

$$Re_c = \rho c V_\infty / \mu = c V_\infty / \nu$$

For wind turbines, Mach numbers are low and this becomes

$$C_i = \text{function}(\text{shape}, \alpha, Re_c); \quad i = p, f, l, d, m$$

For wind turbines, effects of free-stream turbulence and surface contamination may also become very important – whereas both effects are rather small for typical aeronautical applications.

Boundary layer separation and stall

It is obvious that $C_l = 0$ when $\alpha = \pi/2$ (90 deg).

But nonlinear/boundary layer effects make C_l reach a turning point at much lower α, called the stall angle of attack.

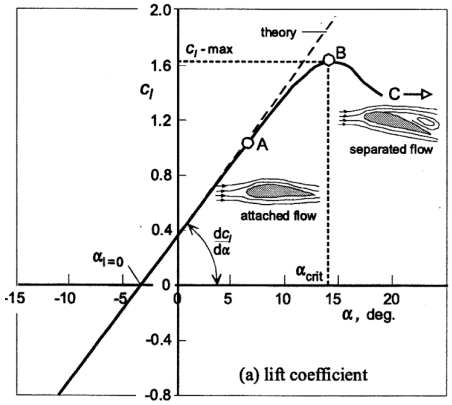

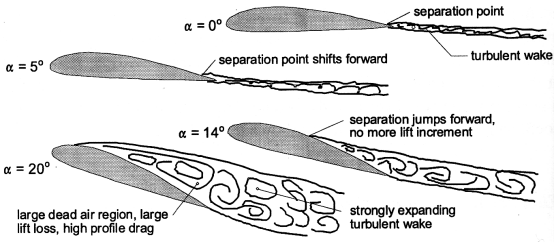

Torenbeek & Wittenberg

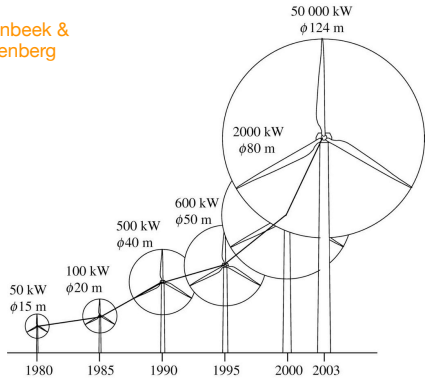

The details of how this happens, and of the aerodynamic coefficients in general, are quite strong functions of *Re* over ranges typical for wind turbine operation.

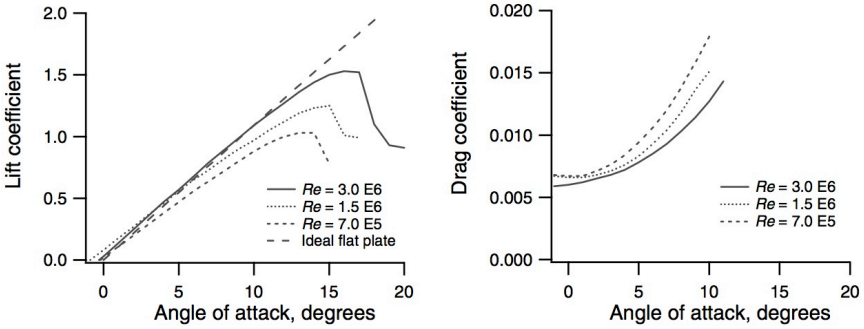

Data for NACA 0012 airfoil, Manwell et al.

Power	*Re* root	*Re* tip
0.2 kW	5.8×10^4	1.2×10^5
50 kW	2.0×10^5	1.3×10^6
600 kW	7.0×10^5	1.3×10^6
2 MW	1.5×10^6	2.2×10^6

Post-stall behaviour

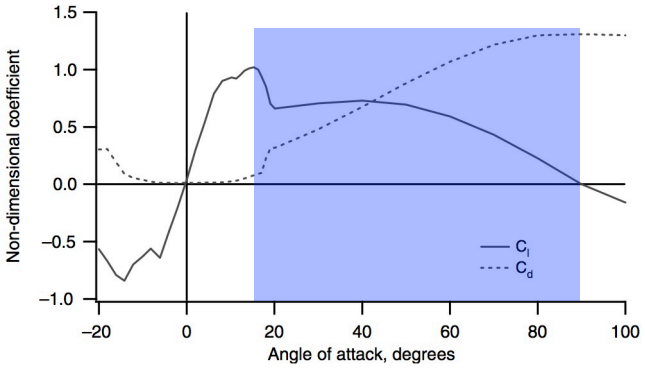

Manwell et al.

More than is commonly the case in aeronautical applications, portions of wind turbine rotor blades may be stalled for significant parts of operation, e.g. during starting or for speed regulation.

Hence information about post-stall behavior is often required but can be difficult to obtain from database sources.

And it is difficult to model computationally. Various simplified models exist for static estimates.

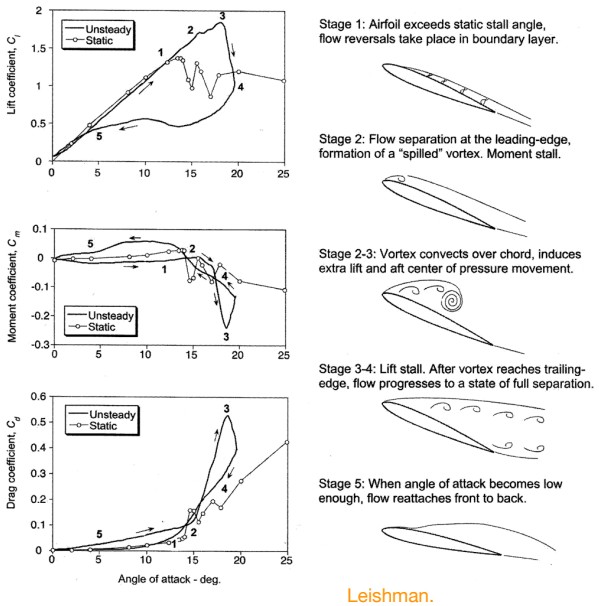

Leishman.

More generally, blades may stall and then recover during different rotation phases. This leads to the need for data or models of dynamic stall behaviour, which is typically hysteretic.

Finite lifting wings (and blades) trail vortices behind

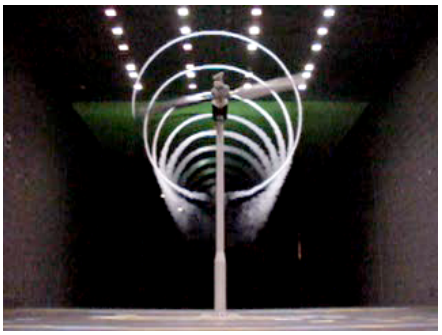

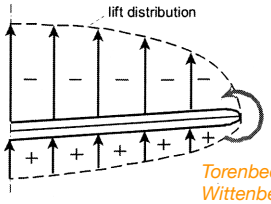

(a) Flow around the tips (front view)

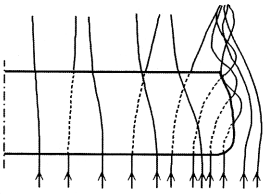

(b) Cross flow (top view)

Wing-tip vortices are driven by pressure differential between the upper and lower sides of a wing, associated with production of lift.

An alternative viewpoint in terms of circulation is that the swirl cannot abruptly end at wing/blade tips - it has to trail downstream.

1: Pressure difference AND lift (circulation) per unit span must fall to zero at wing/blade tips.

2. A downwash velocity is produced by tip vortices.

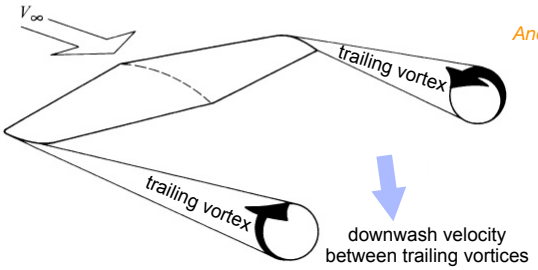

van Dyke

Side view

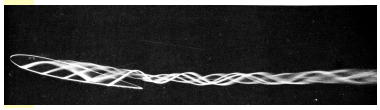

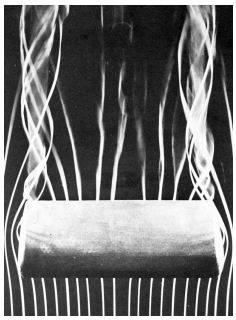

Wind turbines: tip and root vortices

For a wind turbine (or propeller) blade circulation must be shed from both the root and tip of each blade in a helical arrangement.

As for a finite wing, this is related to the fall in circulation aligned along the blade to zero at each end, owing to a reduction in pressure difference from one side of the blade to the other to zero at each blade end.

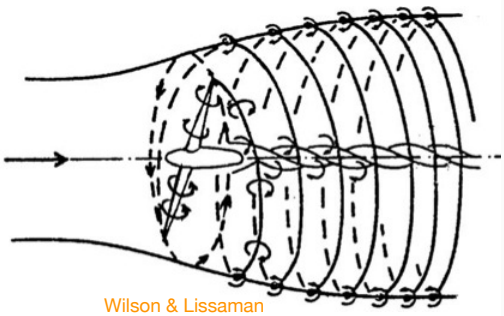

Wilson & Lissaman

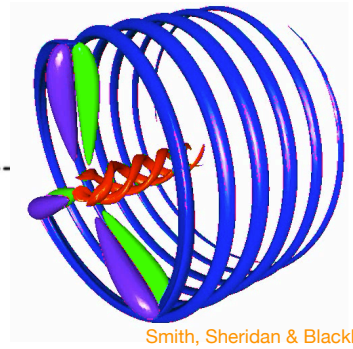

Smith, Sheridan & Blackburn

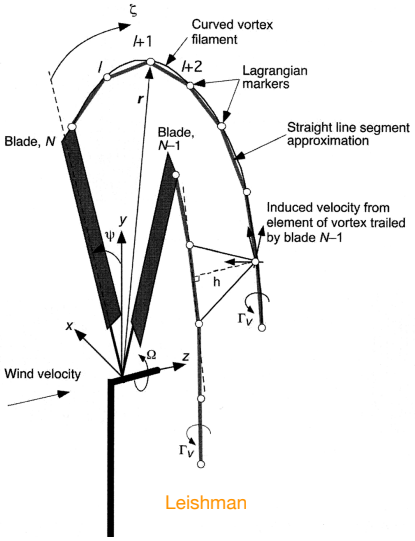

Leishman

This must produce yet another source of induced velocity (and associated losses) to be considered in blade analysis, but the analysis is considerably more complicated than usually used in wing aerodynamics owing to the complex shapes involved.

The usual approach is to use a 'tip loss correction', as initially worked out by Prandtl. While not completely accurate it is often assessed as being 'accurate enough' for turbine design purposes.

Blade element momentum (BEM) method

This method is a hybrid of the 1D actuator disk with swirl analysis with localised analysis accounting for a finite number of blades of given chord, airfoil section and twist.

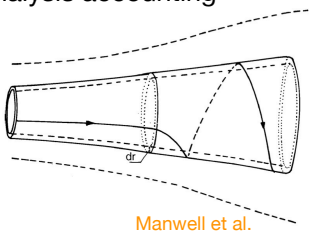

Manwell et al.

1. The stream tube is broken down into a number of annular elements.
2. There is no radial flow across these element boundaries.
3. There is assumed to be no radial dependency; the flow within each element is independent.
4. The force from the blades on the flow is constant in each annular element - the number of blades is initially assumed infinite.
5. Correction for a finite number of blades is made via Prandtl's tip loss factor.

For an annular streamtube with swirl, we already established the infinitesimal contributions to overall

Thrust $\mathrm{d}T = 4a(1-a)\frac{1}{2}\rho V_\infty^2 2\pi r\,\mathrm{d}r$

Torque $\mathrm{d}Q = 4\pi\rho\Omega V_\infty a'(1-a)r^3\,\mathrm{d}r$ at each radius *r*.

Power $\mathrm{d}P = \Omega\,\mathrm{d}Q = 4\pi\rho\Omega^2 V_\infty a'(1-a)r^3\,\mathrm{d}r$

Velocity triangle and blade geometry at a given *r* :

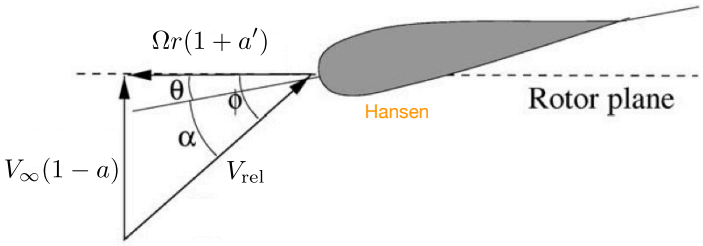

α = (local) blade angle of attack

θ = (local) blade pitch angle
= $\theta_p + \beta$
= (reference/tip) pitch angle, θ_p
+ blade twist angle, β

Blade element momentum (BEM) method

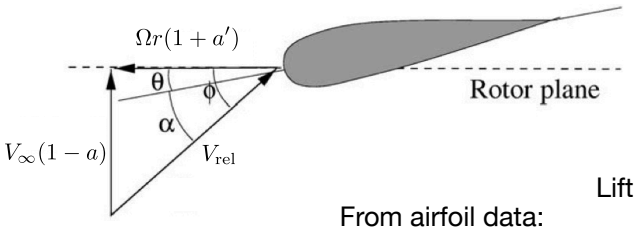

Geometry:

$$\alpha = \phi - \theta$$

$$\tan\phi = \frac{(1-a)V_\infty}{(1+a')\Omega r}$$

From airfoil data:

Lift force per unit length $L = \frac{1}{2}\rho V_{\mathrm{rel}}^2\, c\, C_l(\alpha)$

Drag force per unit length $D = \frac{1}{2}\rho V_{\mathrm{rel}}^2\, c\, C_d(\alpha)$

But we care more about these forces resolved into directions tangential and normal to the rotor plane.

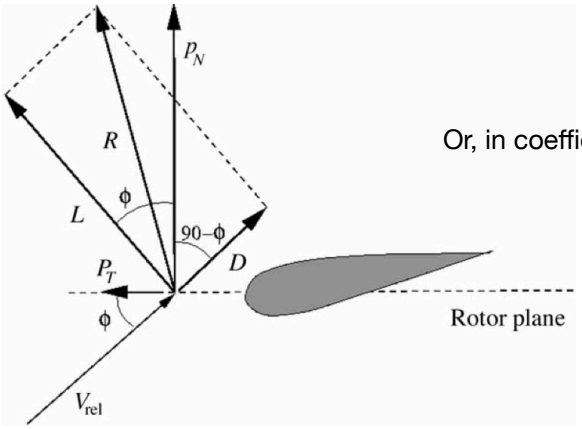

$$p_T = L\sin\phi - D\cos\phi$$

$$p_N = L\cos\phi + D\sin\phi$$

Or, in coefficient form $C_t = C_l\sin\phi - C_d\cos\phi = \dfrac{p_T}{\frac{1}{2}\rho V_{\mathrm{rel}}^2 c}$

$$C_n = C_l\cos\phi + C_d\sin\phi = \frac{p_N}{\frac{1}{2}\rho V_{\mathrm{rel}}^2 c}$$

From geometry $V_{\mathrm{rel}}\sin\phi = V_\infty(1-a)$

$$V_{\mathrm{rel}}\cos\phi = \Omega r(1+a')$$

We define the solidity $\sigma(r) = \dfrac{c(r)B}{2\pi r}$ where *B* is number of blades.

Blade element momentum (BEM) method

Now combining terms we have alternative expressions for infinitesimal contributions to thrust and torque:

$$\mathrm{d}T = B\,p_N\,\mathrm{d}r = \tfrac{1}{2}\rho B\frac{V_\infty^2(1-a)^2}{\sin^2\phi}c\,C_n\,\mathrm{d}r$$

$$\mathrm{d}Q = rBp_T\,\mathrm{d}r = \tfrac{1}{2}\rho B\frac{V_\infty(1-a)\Omega r(1+a')}{\sin\phi\cos\phi}c\,C_t\,\mathrm{d}r$$

Equating with $\mathrm{d}T = 4a(1-a)\tfrac{1}{2}\rho V_\infty^2 2\pi r\,\mathrm{d}r$ and $\mathrm{d}Q = 4\pi\rho\Omega V_\infty a'(1-a)r^3\,\mathrm{d}r$, rearranging, we obtain:

$$a = 1/\left[(4\sin^2\phi)/(\sigma C_n)+1\right] \qquad a' = 1/\left[(4\sin\phi\cos\phi)/(\sigma C_t)-1\right]$$

A solution algorithm for each strip (radius *r*) given blade geometry, *Ω*, and V_∞ is then

1. Intialise *a* and *a'*, typically *a* = *a'* = 0.
2. Compute the local flow angle ϕ. $\phi = \arctan\{[(1-a)V_\infty]/[(1+a')\Omega r]\}$
3. Compute the local angle of attack, α. $\alpha = \phi - \theta$
4. Obtain C_l and C_d from tabulated values.
5. Compute C_n and C_t. $C_n = C_l\cos\phi + C_d\sin\phi \qquad C_t = C_l\sin\phi - C_d\cos\phi$
6. Compute *a* and *a'*. $a = [(4\sin^2\phi)/\sigma C_n + 1]^{-1} \quad a' = [(4\sin\phi\cos\phi)/\sigma C_t - 1]^{-1}$
7. Have *a* and *a'* converged? (No → return to step 2)
8. Compute the local loads on the blade segment.

Since flows at each radial location were assumed independent, this algorithm can be used independently at each radius.

We still need to apply Prandtl's tip loss correction and Glauert's load correction if *a* is large.

Prandtl's tip loss correction factor *F*

Prandtl's tip loss correction – and variations on it – are approximations that attempt to account for the effects of the additional flows induced by the presence of the helical array of tip vortices (at each end of the blade).

Prandtl's model is based on the ideal flow around the edges of an array of discs held normal to the oncoming flow. It is a simple approximation but works surprisingly well if tip speed ratios are not too small.

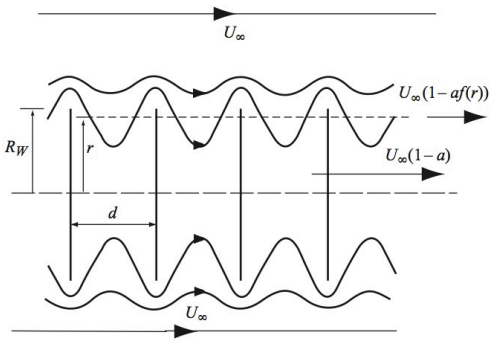

Burton et al.

The tip loss factor *F* is applied to the infinitesimal contributions to thrust, torque and power coefficients

$$\mathrm{d}T = F\,4\pi r\rho V_\infty^2 a(1-a)\,\mathrm{d}r$$

$$\mathrm{d}Q = F\,4\pi r^3\rho V_\infty\Omega a'(1-a)\,\mathrm{d}r$$

$$\mathrm{d}P = F\,4\pi r^3\rho V_\infty\Omega^2 a'(1-a)\,\mathrm{d}r$$

$$F = \frac{2}{\pi}\cos^{-1}\exp(-f) \quad \text{with} \quad f = \frac{B}{2}\frac{1-(r/R)}{(r/R)\sin\phi}$$ Blade tip

$$\text{or} \quad f = \frac{B}{2}\frac{(r/R)-(R_0/R)}{(r/R)\sin\phi}$$ Root @ R_0

If accounting for both root and tip losses then $F = F_{\text{tip}} \times F_{\text{root}}$

The loss factor *F* is incorporated into the BEM method by changing the definitions of the axial and azimuthal induction factors as follows:

$$a = 1/\left[(4F\sin^2\phi)/(\sigma C_n)+1\right]$$

$$a' = 1/\left[(4F\sin\phi\cos\phi)/(\sigma C_t)-1\right]$$

Glauert loading correction for large *a*

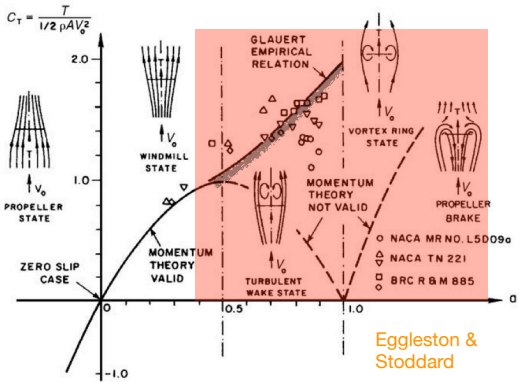

It is found that the assumptions of simple momentum theory break down for $a > 0.4$.

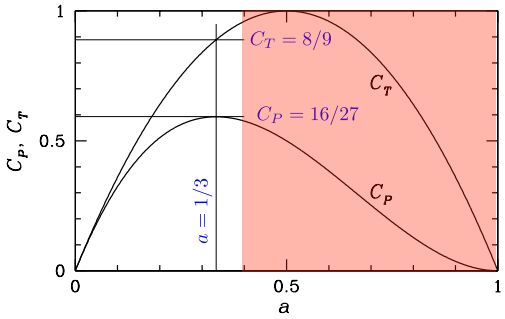

The response is to adopt empirical relations for C_T at large values of *a*.

$$C_T = \underset{\text{Glauert}}{\begin{cases} 4a(1-a)F & a \le 1/3 \\ 4a[1-0.25(5-3a)a]F & a > 1/3 \end{cases}} \quad \text{or} \quad C_T = \underset{\text{Spera}}{\begin{cases} 4a(1-a)F & a \le a_c \\ 4[a_c^2 + (1-2a_c)a]F & a > a_c \end{cases}} \qquad a_c \approx 0.2$$

The second of these gives

$$a = 1/\left[(4F\sin^2\phi)/(\sigma C_n) + 1\right] \qquad a \le a_c$$

$$a = 0.5\left[2 + K(1-2a_c) - \sqrt{[K(1-2a_c)+2]^2 + 4(Ka_c^2 - 1)}\right] \qquad a > a_c$$

and $K = (4F\sin^2\phi)/(\sigma C_n)$

The remainder of the BEM method remains as previously described.

BEM evaluation of total load, torque and power

Given a HAWT rotor geometry and V_∞, Ω, we are now able to use BEM method to calculate the thrust load and torque (and hence power) for the whole rotor by integration:

Thrust $T = \int_{R_0}^{R} \frac{\mathrm{d}T}{\mathrm{d}r}\,\mathrm{d}r$ Torque $Q = \int_{R_0}^{R} \frac{\mathrm{d}Q}{\mathrm{d}r}\,\mathrm{d}r$ Power $P = \Omega Q$

using the expressions already established for d*T*/d*r* and d*Q*/d*r*.

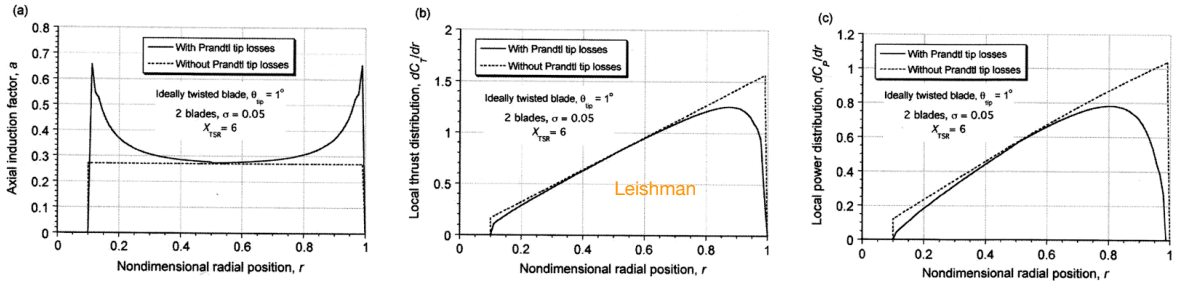

If desired we could then work back to obtain

$$C_T = \frac{T}{\frac{1}{2}\rho A V_\infty^2} = \frac{2T}{\pi R^2 \rho V_\infty^2} \qquad C_P = \frac{P}{\frac{1}{2}\rho A V_\infty^3} = \frac{2P}{\pi R^2 \rho V_\infty^3}$$

for one value of $\lambda = \frac{\Omega R}{V_\infty}$

Repeat the same calculations for a range of λ values (to cover the expected range of V_∞ if Ω is fixed, say).

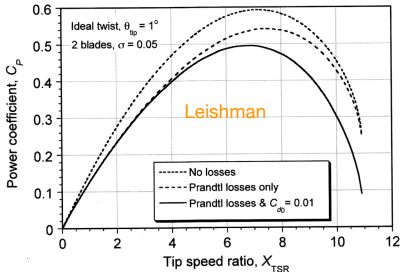

Finally, if we have PDF of wind speed, $p(V_\infty)$:

$$\overline{P} = \int_0^\infty P(V_\infty)\, p(V_\infty)\, \mathrm{d}V_\infty$$

BEM evaluation of total load, torque and power

Finally we should point out that larger wind turbines often operate near a fixed rotational speed Ω, determined by the grid AC frequency (e.g. 50 Hz), the generator design, and mechanical gearbox.

In this case it is useful to plot the dimensionless performance characteristics in the form of a K_P vs 1/λ curve. This shows (non-dimensionally) how the power output varies with wind speed for a fixed rotational speed.

$$K_P = \frac{\text{Power}}{\frac{1}{2}\rho(\Omega R)^3 A_D} = \frac{\text{Power}}{\frac{1}{2}\rho(\Omega R)^3 \pi R^2} = \frac{C_P}{\lambda^3} \qquad 1/\lambda = \frac{V_\infty}{\Omega R} \propto V_\infty$$

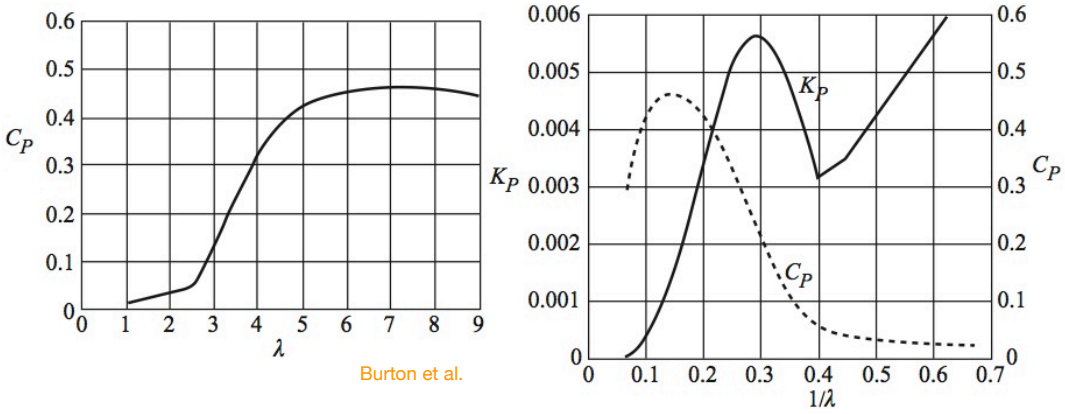

Burton et al.

Electrical generator characteristics

The most common type of electrical generator for large wind turbines connected to a 3-phase AC power grid is the asynchronous induction generator. These have a multi-bar 'squirrel cage' rotor connected to the shaft and a rotating magnetic field generated by each of the phases hooked up to separate electromagnet coil in the stator, producing a rotating magnetic field (RMF). Each set of three coils constitutes a single magnetic dipole.

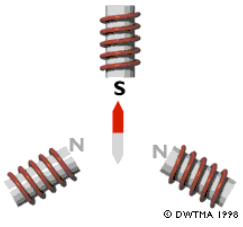

Two-pole stator

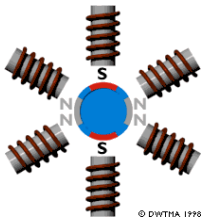

Four-pole stator

The speed of rotation of the magnetic field reduces as the number of pole pairs increases.

Most common

No. of poles	Synchronous speed (rpm)
2	3000
4	1500
6	1000
8	750

A step-up gearbox is used between the turbine shaft and the generator shaft.

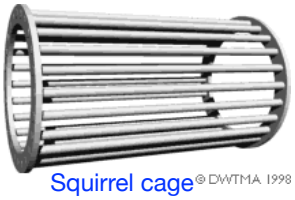

Squirrel cage © DWTMA 1998

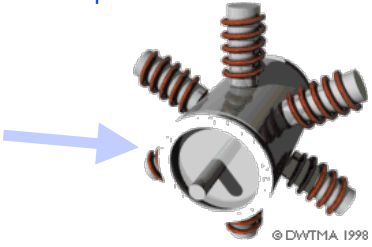

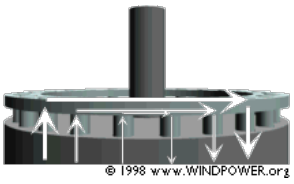

If the squirrel cage/generator shaft rotates at the same speed as the RMF there is no torque and no current flows in the squirrel cage bars. If the shaft rotates at a slightly higher speed then a large current will flow in the cage, producing its own magnetic field, which in turn interacts with the magnetic field in the stator to generate a back-EMF in the stator windings. (Alternatively, if the shaft rotates slower, we have a motor.)

http://www.motiva.fi/myllarin_tuulivoima/windpower%20web/core.htm

Electrical generator characteristics

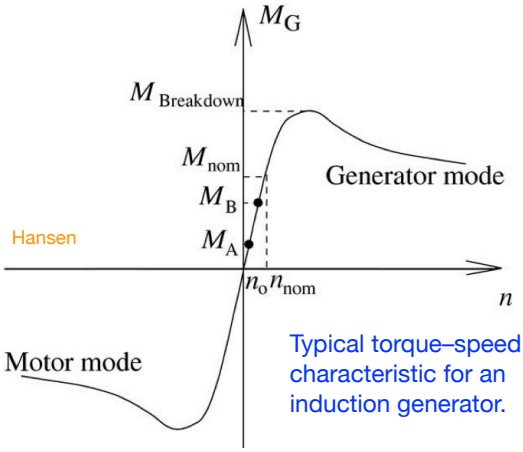

Hansen

Typical torque–speed characteristic for an induction generator.

$$n_0 = 60\frac{f_{grid}}{\text{No. of poles}}$$ (f_{grid} in Hz, n_0 in RPM)

$$\text{Slip} = \frac{n - n_0}{n_0}$$ Typically 1 – 3%.

$$n = \frac{\Omega}{2\pi} \times \text{gearbox ratio}$$

The torque–speed characteristic of the turbine is set so that (referred to the generator through the gearbox ratio) the two torques balance in the linear portion of the curve, below the breakdown (a.k.a. pullout) torque and where the electrical efficiency is reasonable.

For a stall-regulated turbine, the generator can be used in motor mode to spin the disk up to synchronous speed.

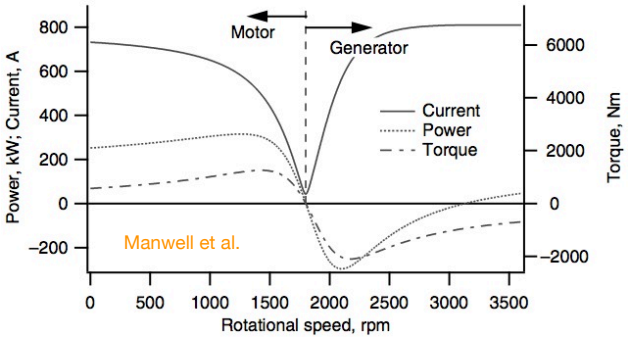

Manwell et al.

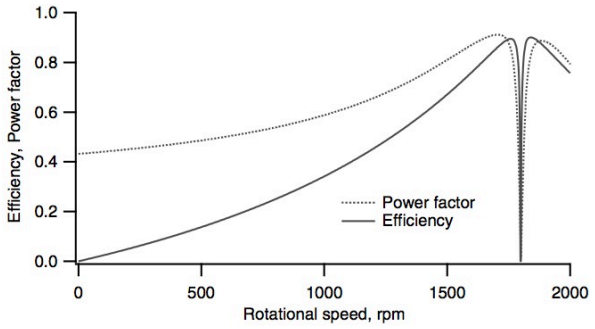

NB: these two diagrams are for a 60 Hz grid frequency and a 4-pole stator.

Aerodynamic aspects of control

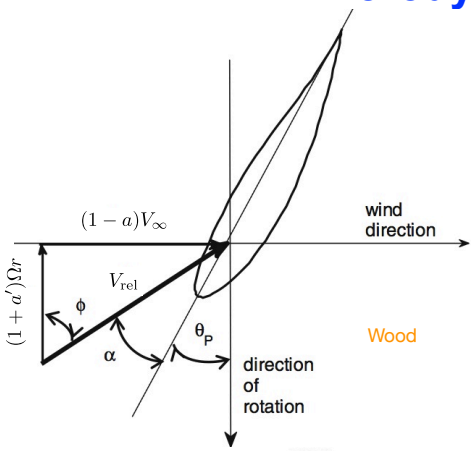

Wood

It is easy enough to see that for any given pitch angle θ_p and rotational speed Ω, at least some part of the blade will stall as wind speed V_∞ increases (i.e. as a increases).

1. For fixed pitch, the blade is likely to be completely stalled at $\Omega = 0$. This may mean the turbine is not self-starting – an important design consideration especially for small machines.
2. For fixed pitch and a given rotational speed Ω, the blade will eventually become completely stalled as $V_\infty \to \infty$. This can aid in regulating power output to the rated value of the electrical generator at high wind speeds, since for large machines the rotational speed is usually approximately fixed.
3. Variable pitch may be used actively on the entire blade as part of the starting/power regulation system, or passively at the blade tip for braking/power regulation.

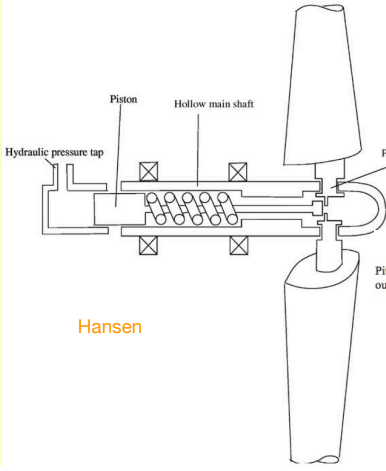

Hansen

Burton et al.

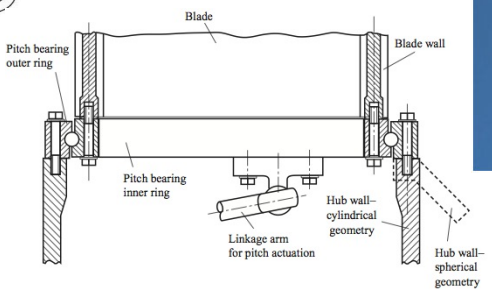

Aerodynamic aspects of control

BEM calcs for NTK 500/41 fixed-pitch stall-regulated turbine, rotational speed 26.8 RPM (= 1500/56 RPM).

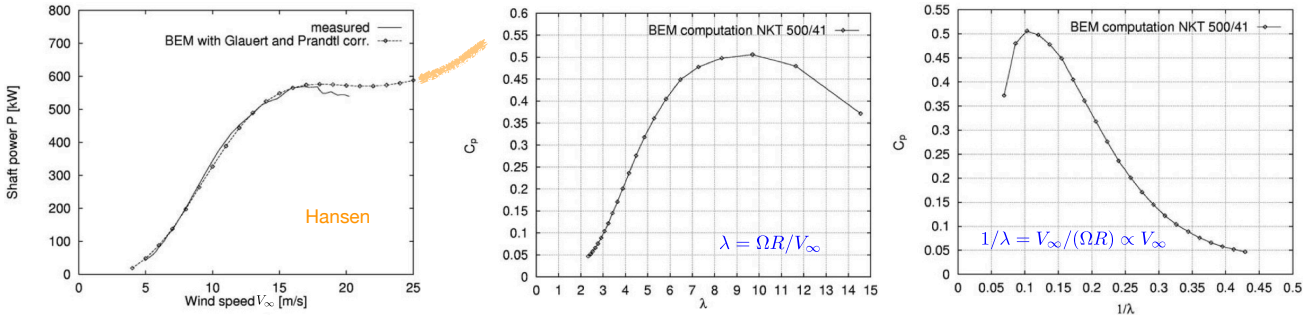

Typically, fixed-pitch machines must be started using a motor once the cut-in speed is reached, and are braked either aerodynamically or mechanically above an upper-limit speed (for the turbine above, these two wind speeds are 4 m/s and 25 m/s respectively). (NB: blade pitch can be manually adjusted at the hub.)

For variable-pitch (but constant nominal speed) wind turbines, the pitch is controlled so that above a particular wind speed the rated power of the generator is matched and the aerodynamic power becomes independent of wind speed.

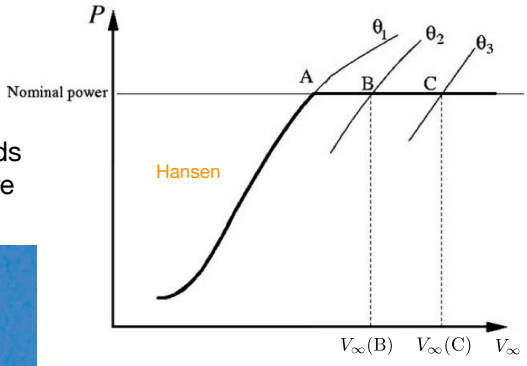

Variable pitch turbines can be made self-starting low wind speeds and either feather- or stall-regulated at high speeds. But they are more complex than fixed-pitch machines.

Small wind turbines may also use yaw control for furling (shut-down) at high wind speeds.

Aerodynamic aspects of control

1 MW machine run with fixed pitch and stall regulation.

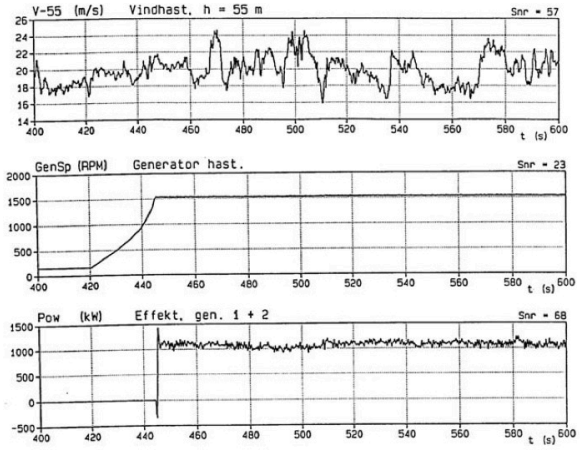

Same turbine run as a variable-pitch machine.

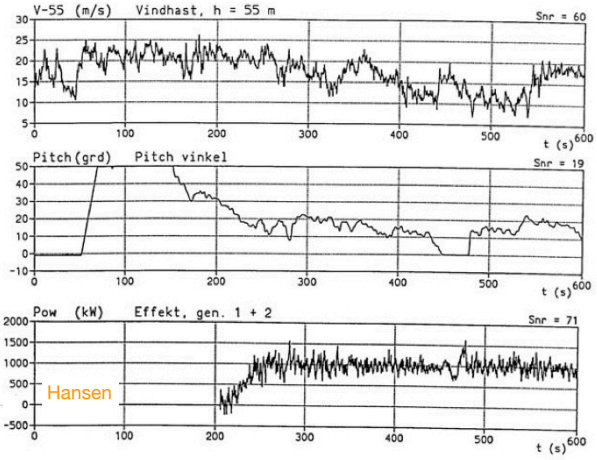

Pitch-regulated turbines have a larger values of dP/dV_∞ than equivalent stall-regulated turbines when running at rated power and hence show greater variation in power output with wind-speed fluctuation.

However they have lower fluctuating structural loads and can continue operation in higher wind speeds than an equivalent stall-regulated turbine.

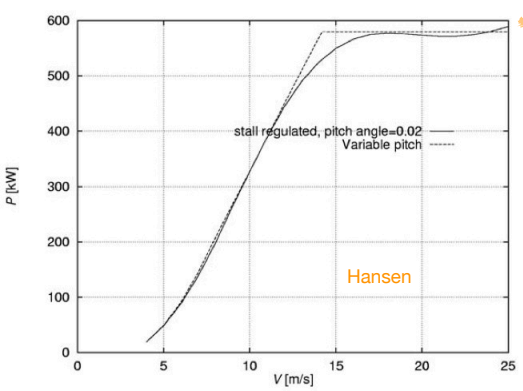

Aerodynamic aspects of control

For variable-pitch machines there are two ways of achieving control to regulate power to the rated value of the generator. The two sets of curves below are for a 60 kW turbine/generator combination.

1. Pitching to stall

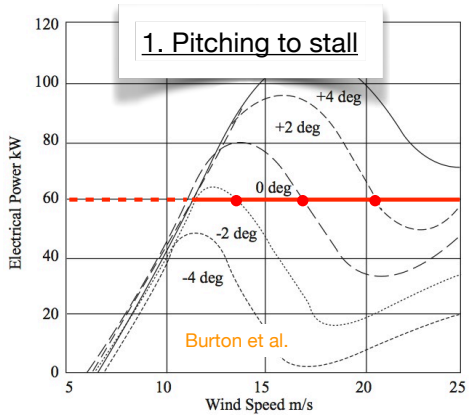

2. Pitching to feather

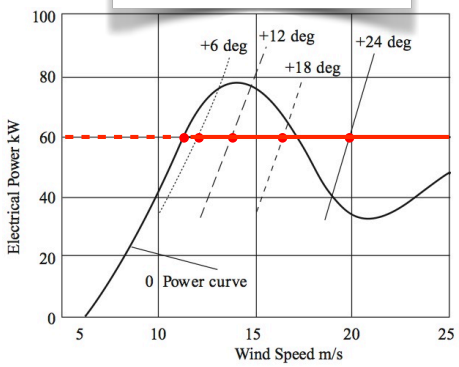

'Pitching to stall' involves small pitch angle excursions but there is some upper wind speed at which that method is unable to maintain control and external braking must be applied.

'Pitching to feather' involves large pitch angle excursions but is able to maintain control at all wind speeds. A disadvantage is that the instantaneous power output becomes increasingly sensitive to wind speed fluctuation.

The two options can be plotted on a control-strategy diagram. Below the bifurcation, pitch is set to optimise power output for each wind speed.